PIEZOELECTRICS

Induced giant piezoelectricity in centrosymmetric oxides

D.-S. Park[1,2]*, M. Hadad[2], L. M. Riemer[1], R. Ignatans[3], D. Spirito[4], V. Esposito[5], V. Tileli[3], N. Gauquelin[6,7], D. Chezganov[6,7], D. Jannis[6,7], J. Verbeeck[6,7], S. Gorfman[4], N. Pryds[5], P. Muralt[2], D. Damjanovic[1]*

Piezoelectrics are materials that linearly deform in response to an applied electric field. As a fundamental prerequisite, piezoelectric materials must have a noncentrosymmetric crystal structure. For more than a century, this has remained a major obstacle for finding piezoelectric materials. We circumvented this limitation by breaking the crystallographic symmetry and inducing large and sustainable piezoelectric effects in centrosymmetric materials by the electric field–induced rearrangement of oxygen vacancies. Our results show the generation of extraordinarily large piezoelectric responses [with piezoelectric strain coefficients (d_{33}) of ~200,000 picometers per volt at millihertz frequencies] in cubic fluorite gadolinium-doped CeO_{2-x} films, which are two orders of magnitude larger than the responses observed in the presently best-known lead-based piezoelectric relaxor–ferroelectric oxide at kilohertz frequencies. These findings provide opportunities to design piezoelectric materials from environmentally friendly centrosymmetric ones.
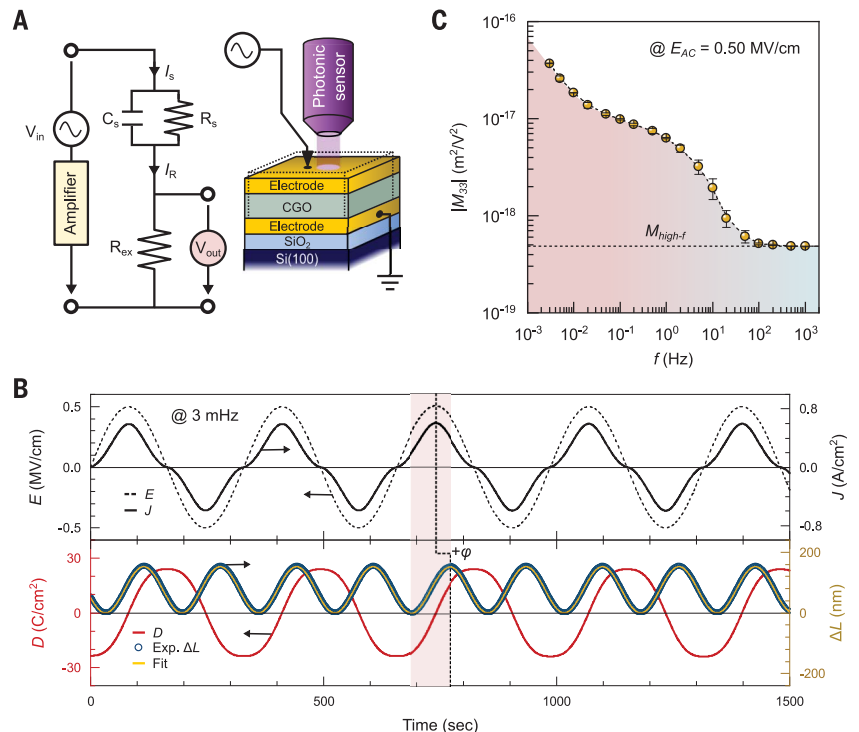
The fundamental principle of electrostriction and piezoelectric effects stems from small deformations of the crystal unit cell by an applied electric field. The latter effect also provides charge separation under mechanical pressure (1). The associated displacements of atoms are in the picometer range, so atoms remain confined around their original crystallographic sites. Piezoelectricity is of high technological and industrial importance and is used in a vast number of applications, such as medical devices, actuators, and sensors (2). Motivations to augment the piezoelectric response, which requires materials with a noncentrosymmetric structure, are therefore compelling. Among piezoelectric materials, perovskite-type oxides are the most widely used and exhibit excellent piezoelectric responses. Several routes to achieve the highest electromechanical response in these materials have been pursued, including control of the material's structural instability at specific chemical compositions (e.g., morphotropic phase boundary) and associated polarization rotation and domain engineering (3), chemical disorder (4), and nanocomposite structures (5). All of these strategies demonstrate the possibility for improving the piezoelectric response within an order of magnitude with respect to that of the industrial standard, $Pb(Zr,Ti)O_3$ (PZT) (6).

The piezoelectric effect can be induced in centrosymmetric materials by applying a direct electric field that breaks the inversion symmetry (7, 8). This approach has been revived recently by applying asymmetric electrodes on centrosymmetric samples, creating different Schottky barriers at the electrodes (9). This approach has the potential to widen the number of prospective electromechanical materials beyond the traditionally dominating ferroelectric lead-based perovskites, but the resulting response is still one to two orders of magnitude lower than that of PZT. Another attempt to induce the effect suggests using the electric field–assisted exchange

[1]Group for Ferroelectrics and Functional Oxides, Swiss Federal Institute of Technology–EPFL, 1015 Lausanne, Switzerland. [2]Group for Electroceramic Thin Films, Swiss Federal Institute of Technology–EPFL, 1015 Lausanne, Switzerland. [3]Institute of Materials, Swiss Federal Institute of Technology–EPFL, 1015 Lausanne, Switzerland. [4]Department of Materials Science and Engineering, Tel Aviv University, Ramat Aviv, Tel Aviv 6997801, Israel. [5]Department of Energy Conversion and Storage, Technical University of Denmark, Fysikvej, 2800 Kongens Lyngby, Denmark. [6]Electron Microscopy for Materials Science (EMAT), University of Antwerp, B-2020 Antwerpen, Belgium. [7]NANOlab Center of Excellence, University of Antwerp, 2020 Antwerp, Belgium.
*Corresponding author. Email: dspark1980@gmail.com (D.-S.P.); dragan.damjanovic@epfl.ch (D.D.)

Fig. 1. Electric field–induced electrostrictive responses of CGO film. (**A**) Schematics of the experimental setup, which combines electrical and electromechanical measurements for the CGO samples. The equivalent circuit shows the voltage source, V_{in}; the voltage amplifier; the CGO capacitor, C_S, with resistance, R_S; an external resistor, R_{ex}; the current, I_R, flowing through R_{ex} and the sample; and the output voltage, V_{out}, across R_{ex}. (**B**) Electrical and electromechanical outputs: (i) the applied E_{AC} = 0.5 MV/cm at f = 3 mHz (dashed line), (ii) the corresponding J (solid line), (iii) the derived charge density D (red solid line), and (iv) the concurrently measured second harmonic electromechanical response ΔL of the samples (blue circle in lower panel). The measured ΔL in time was fitted by $\Delta L = L_0 \sin^2(\omega t + \phi)$ as depicted by the solid yellow line. (**C**) Frequency-dependent M_{33} of the CGO film, excited by E_{AC} = 0.5 MV/cm.

of oxygen with the ambient atmosphere in oxygen-nonstoichiometric fluorite structures (Y-doped ZrO_2 or Re^{+3}-doped CeO_2, where Re is a rare earth element) (10). The oxygen exchange (release) results in chemical expansion of the films, leading to bending of thin materials and thus the strain–electrical field (x versus E) relationship, which mimics the piezoelectric effect. The strains achieved are comparable to those in PZT. The field-induced motion of charge carriers takes place over a long range (size of the sample), and the effect is large only at high temperatures (>500°C) and low frequencies (below ~1 Hz), where ionic diffusion is sufficiently large. Additionally, some fluorite oxides (e.g., doped CeO_2) were reported to exhibit electrostrictive coefficients that are about two orders of magnitude higher than expected values from phenomenological relations between electrostrictive coefficient and elastic and dielectric susceptibilities (11). The origin of this large electrostriction has not yet been entirely elu-cidated, but the electric field–induced mechanical deformation is certainly related to the presence and short-range motion of oxygen vacancies (12–14).

We demonstrate a paradigm shift for achieving large, electric field–induced piezoelectricity in centrosymmetric materials. We show that for Gd-doped CeO_{2-x} (CGO) films, which have a cubic fluorite centrosymmetric structure, we can achieve very high values of the electric field–induced piezoelectric strain (x ~ 26%) and apparent longitudinal piezoelectric coefficients (d_{33} of ~200,000 pm/V). This latter value, measured in the millihertz range, is two to three orders of magnitude larger than that observed in the best piezoelectric perovskite oxides—e.g., $Pb(Mg_{1/3}Nb_{2/3})O_3$-$PbTiO_3$ with $d_{33} \approx 2000$ pm/V (3). Notably, and relevant for applications, the induced effect is comparable to that in the best PZT thin films (~100 pm/V) in the kilohertz range (15). We argue that the change in the strain mechanism from the short-range lattice or ionic defect–based mechanism above 10 Hz to the one at low frequencies, is based on distinct actions of the long-range migration of ions (oxygen vacancies, V_O) and electrons. Our results show that the electric field–induced redistribution of mobile charges in the films leads to crystal phase transition, associated with chemical expansion, and material heterogeneity. These combined effects result in giant piezoelectric and electrostrictive responses and point toward a previously unknown electromechanical mechanism in centrosymmetric fluorites and materials with large ionic and electronic conductivity in general.

We deposited polycrystalline $(Gd_{0.2}Ce_{0.8})O_{2-x}$ films on $Al/SiO_2/Si(100)$ substrate at room temperature by sputter deposition (Fig. 1A). The CGO films had thicknesses in the range of ~1.25 to ~1.8 μm (fig. S1) (16). The electrostrictive strain for a sample of length L is defined as
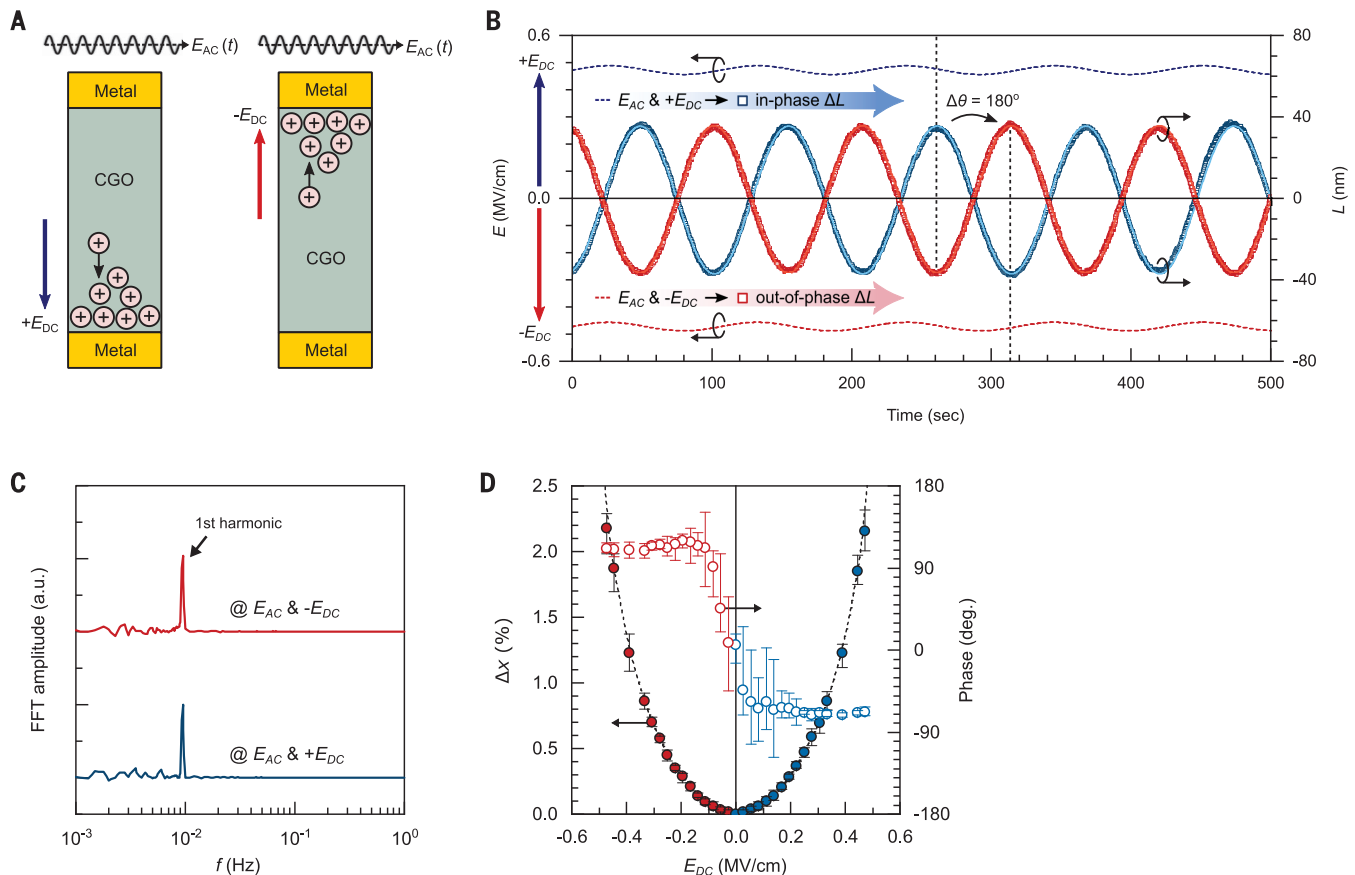
$$x = \Delta L/L = ME^2 \quad (1)$$

Fig. 2. The induced piezoelectric displacements in CGO films. (**A**) A schematic for the electric field application to CGO film in out-of-plane capacitor geometry, which is simultaneously composed of a small driving AC field (E_{AC}) and a large static DC field (E_{DC}). The induced in-phase strain (x_{33}) in the film is determined by the polarity of the applied DC bias. (**B**) Time-resolved first harmonic electromechanical displacements of the CGO film, measured at ~10 mHz (9.4 mHz) and excited by E_{AC} =15.71 kV/cm under E_{DC} = ±0.47 MV/cm. The polarity of the DC field switches the sign of the piezoelectric coefficient. The measured ΔL in time was fitted by the first-order sine function, $\Delta L = L_0 \sin(\omega t - \phi)$, as depicted by the solid red and blue lines. (**C**) The corresponding fast Fourier transform (FFT) amplitude spectra of the generated first harmonic displacements as a function of frequency. a.u., arbitrary units. (**D**) Variations in the x_{33} and response phase angle of the film as a function of DC field while applying a constant E_{AC} (15.71 kV/cm).

where x is the out-of-plane strain of the film, ΔL is the thickness change, M is the corresponding electrostrictive coefficient, and E is the alternated electric field (AC, alternating current) applied between the film's top and bottom electrodes. $E = E_{AC}(t) = E_{AC}\sin(2\pi ft)$, where f is the frequency and t is time. We used two different top electrodes, Al (~150 nm) and Pt (~150 nm)/Cr (~20 nm) layers, to study the effect of asymmetric electrodes on the polarization (fig. S2C). Electrical (current density J versus electric field E) and electromechanical (strain x versus E) measurements on the films were performed on out-of-plane capacitor geometry. We measured the strain x using a contactless fiber-optic method (16). We confirmed the electromechanical displacements using another setup with direct contact measurements (supplementary text, section 1). All of the instrumental artifacts and external effects (e.g., bending and Joule heating effects) have negligible influence, and thus the dominant contribution to the induced strain is originated only from the electromechanical response of the films (figs. S2 and S3).

We show the measured ΔL with the second harmonic response and an offset as obtained from $[\sin(2\pi ft)]^2 = \frac{1}{2}[1 - \cos(4\pi ft)]$ (Fig. 1B). We measured the electric current density J through the film simultaneously with the change in the length ΔL and charge density $D = \int J dt$ (Fig. 1B; supplementary text, section 2; and fig. S4B) (16). We performed measurements of electrostriction across a range of frequencies from 3 mHz to 1 kHz. The electrostrictive coefficient M, which we determined using Eq. 1, shows a notably complex frequency dependence (Fig. 1C). This clearly indicates that at least three different contributions to the electrostriction exist in these samples (Fig. 1C and fig. S4). We suggest that the strong rate-dependent contributions to strain can be attributed to the existence of mobile ionic species (V_O) in the CGO film, as implied by a similar behavior in the AC conductivity (figs. S4 and S5).
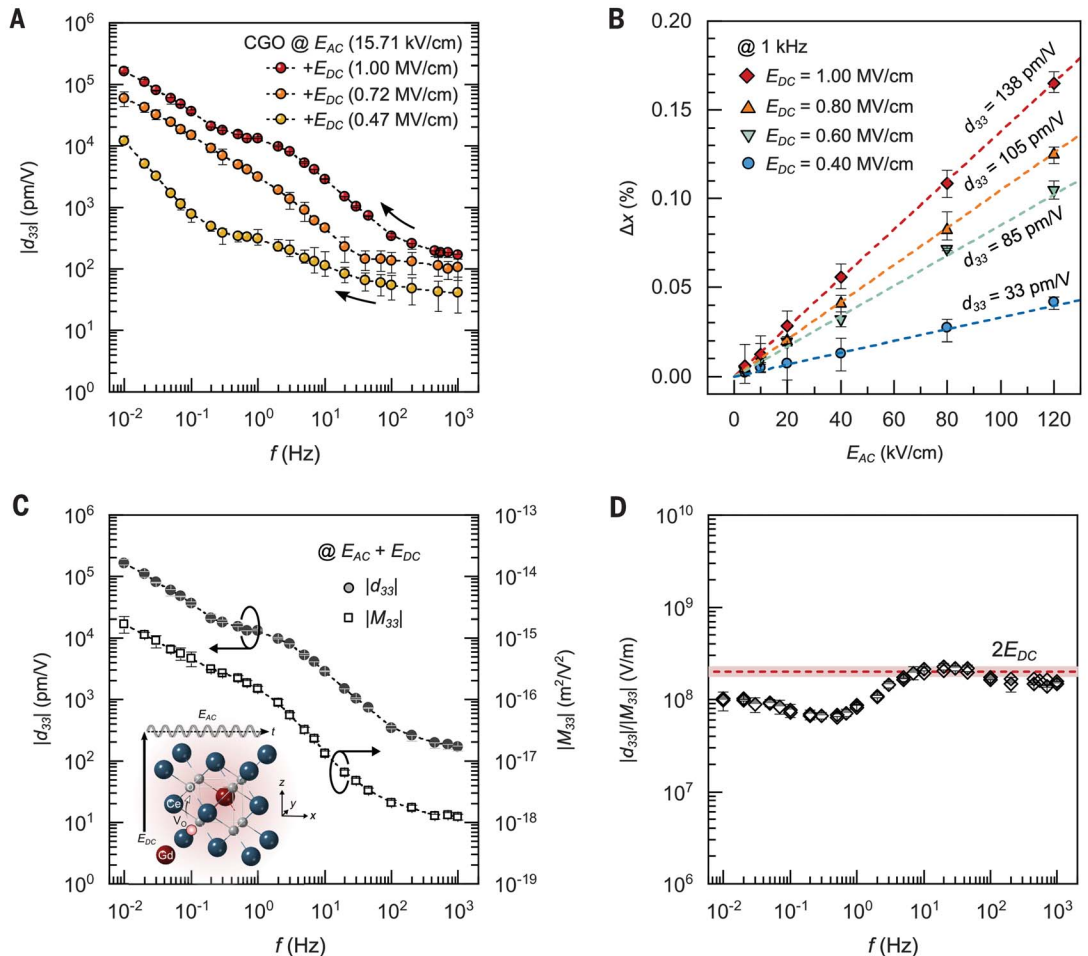
The inversion symmetry in CGO can be broken by applying an electric field bias E_{DC} (DC, direct current), leading to asymmetric charge distribution and induced polarization P_{ind} in the material (Fig. 2A) (1). We can explain this by replacing field E in Eq. 1 with $E = E(t)_{AC} + E_{DC}$

$$x = ME_{DC}^2 + ME_{AC}^2 + (2ME_{DC})E_{AC} \quad (2)$$

The first and second term describe electrostrictive deformations, and the third term is the symmetry-breaking term with the field-induced piezoelectric coefficient, $d_{ind} = 2ME_{DC}$.

The CGO has a centrosymmetric cubic fluorite structure in the ground state and is not piezoelectric. However, we observed the piezoelectric displacement term ($d_{ind} = 2ME_{DC}$) in our CGO films upon application of electric field bias (Fig. 2B) for $E_{DC} = \pm0.47$ MV/cm and $E_{AC} = 15.71$ kV/cm. We observe a clear presence of the first harmonic deformation as well as a 180° phase shift when changing the sign of E_{DC}, which correspond to the induced piezoelectric effect. In this case, we do not observe the electrostrictive displacements (second harmonic) (Fig. 2, B and C) because of a very small amplitude of E_{AC} (compared with E_{AC} in Fig. 1A). Once the E_{AC} is comparable to or higher than E_{DC}, we observed an asymmetric response comprising both the first and the second harmonics (fig. S6). Measuring the piezoelectric strain of the CGO sample as a function of E_{DC} (in the range of ±0.47 MV/cm) while keeping the same electric field E_{AC} (15.71 kV/cm) at 10 mHz clearly shows that the applied E_{DC} tunes the piezoelectric AC

Fig. 3. Frequency-dependent piezoelectric susceptibility of CGO film. (**A**) The first harmonic electromechanical susceptibility $|d_{33}|$ of the CGO film as a function of f (10 mHz ≤ f ≤ 1 kHz), excited by a constant driving AC field ($E_{AC} = 15.71$ kV/cm) and different static DC fields ($E_{DC} = +0.47$, $+0.72$, and $+1.00$ MV/cm). (**B**) Linear piezoelectric strain of the CGO film as a function of E_{AC} with various E_{DC}, measured at 1 kHz. (**C**) $|d_{33}|$ and $|M_{33}|$ of the film, simultaneously measured by applying a combined electric field, $E_{AC} = 15.71$ kV/cm and $E_{DC} = +1.00$ MV/cm, in the frequency range from 10 mHz to 1 kHz. The inset describes the field-enforced defect dynamics, polarization reorientation, and the following permittivity variations in CGO. (**D**) Ratios of $|d_{33}|$ to $|M_{33}|$ as a function of f, expected to be $2E_{DC}$ in the relation of $d_{ind} = 2M_{ind}E_{DC}$.
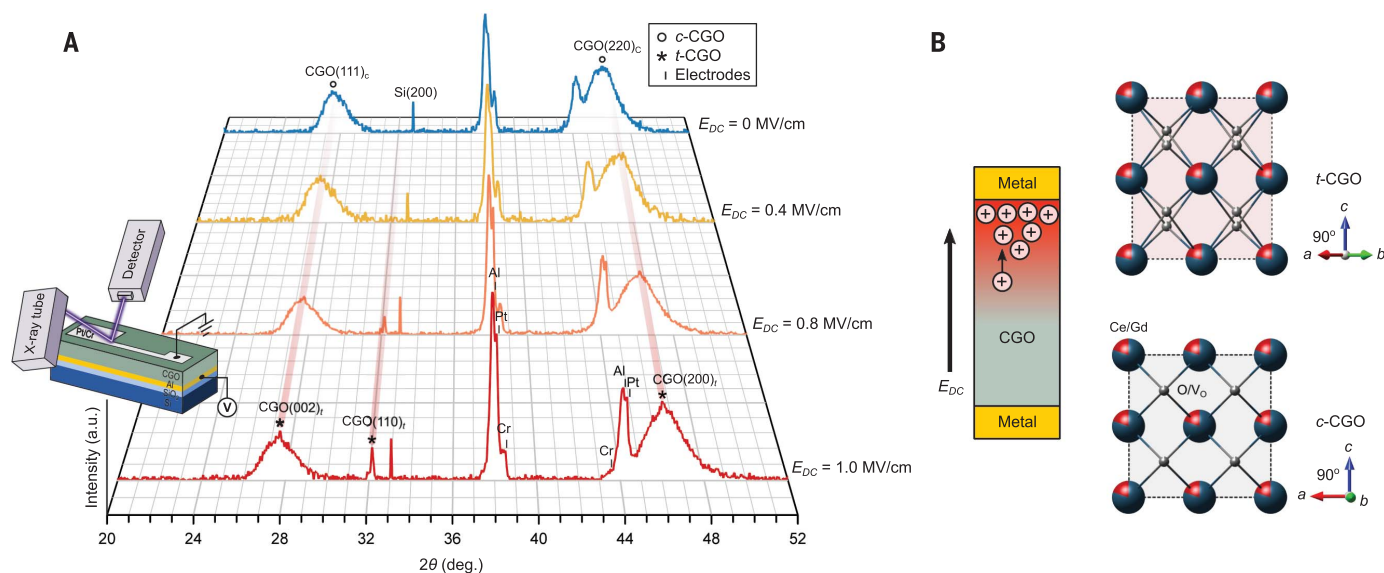
Fig. 4. Effect of V_O redistribution in centrosymmetric fluorite CGO film.
(**A**) XRD 2θ patterns of the polycrystalline CGO film under various in situ E_{DC} applications (0, 0.4, 0.8, and 1.0 MV/cm). Schematic shows the in situ XRD measurement setup using a laboratory-source x-ray (λ = 1.54056 Å) and top electrode area (~10%) at the surface, which was connected to the applied electric fields. Under $E_{DC} \geq 0.8$ MV/cm, diffraction peaks were visible at 2θ = 28.3°, 32.6°, and 46.9°, which are assigned to (002), (110), and (200) reflections of a tetragonal phase of CGO, respectively. (**B**) Schematics for the phase transition of CGO from cubic to tetragonal phase through the field-induced redistribution of mobile positively charged V_O (+).

strain, reaching values of up to 2.15% (d_{ind} ~ 13,700 pm/V) (Fig. 2D). The nonlinear dependence of the AC strain on E_{DC} (Fig. 2D) reflects the fundamental nature of the electrostriction coupling to polarization and not directly to the field. Furthermore, the on-off control of piezoelectricity and electrostriction and the tuning of the electromechanical response can be sustained for at least several hours without any sign of degradation (figs. S7 and S8).

We show the piezoelectric coefficients of the CGO sample, determined as a function of frequency (from 10 mHz to 1 kHz), for different fields E_{DC}—e.g., 0.47, 0.72, and 1.00 MV/cm (Fig. 3A). The results are notable when compared with the frequency-independent response in conventional piezoelectric materials (e.g., PZT) and a bismuth titanate–based ceramic (fig. S9). First, the piezoelectric coefficient reaches giant values at low frequencies, approaching ~200,000 pm/V with increasing E_{DC}. For comparison, the piezoelectric coefficient in the best commercial single crystals of Pb(Mg$_{1/3}$Nb$_{2/3}$)O$_3$-PbTiO$_3$ (PMN-PT) is ~2000 pm/V and is ~200 to 500 pm/V in PZT ceramics (3). Notably, the values around 100 pm/V, measured at 1 kHz in our films, are comparable to those of PZT thin films (15). This is the frequency range of interest for many actuator applications. We observed clear high-f (1 kHz) piezoelectric responses for the CGO film with a linear relation following $x = d_{ind}E_{AC}$, whereas the d_{ind} varies with applied E_{DC}, as expected (Fig. 3B).

Further insight into the electric field–induced piezoelectric response of the CGO can be ob-

tained from the piezoelectric term of Eq. 2, from which one can derive

$$d_{ind} = 2ME_{DC} = 2\varepsilon Q P_{ind} \qquad (3)$$

where ε is the dielectric permittivity; Q is the polarization-related electrostrictive constant, $x = QP_{ind}^2$ (17); $P_{ind} = \varepsilon E_{DC}$ is the induced polarization; and $M = \varepsilon^2 Q$. Equation 3 generally holds very well for centrosymmetric materials—for example, for perovskite relaxors (7) and Schottky barrier–induced piezoelectric effect (9). We show the simultaneously measured piezoelectric and electrostrictive coefficients over a wide frequency range (Fig. 3C). The ratio of $|d|/|M|$ is expected from Eq. 3 to be equal to $2E_{DC}$. We see a good agreement ($|d|/|M| \approx 2E_{DC}$) for $f \geq 10$ Hz (Fig. 3D), whereas the ratio is lower at low frequencies ($f \leq 1$ Hz). Consequently, these data indicate the presence of a rate-dependent mechanism that is triggered by the application of E_{DC} and that is assisted by the application of quasi-static E_{AC} at low frequencies. The relationship $d_{ind} = 2\varepsilon Q P_{ind}$ is considered fundamental and always holds (1, 17) where the polarization response is controlled by small oscillations of ions and electrons near their equilibrium lattice sites. Our results show that good agreement between the calculated and the measured M and d values holds over the frequency range where apparent polarization and permittivity $\left(\varepsilon_{ij} = \frac{\partial P_i}{\partial E_j} \right)$ are dominated by the rate-dependent migration of $V_O^{\bullet\bullet}$ (supplementary text, section 3, and figs. S10

and S11) (16). The introduction of aliovalent dopants, e.g., Gd^{3+} in CeO$_2$, produces negative charges and requires 1/2 oxygen vacancy for maintaining charge neutrality; in Kröger-Vink notation (18), this can be written as Ce$^\times_{0.8-2y}$Ce$'_{2y}$(Gd$'_{Cd}$)$_{0.2}$O$^\times_{1.9-y}$(V$_O^{\bullet\bullet}$)$_{0.1+y}$, where (Gd$'_{Ce}$) = 2(V$_O^{\bullet\bullet}$). The additional oxygen vacancies (y) produced during preparation and charge compensated by Ce^{+3} are arguably more mobile than those associated with Gd (14, 19), at least at weaker fields. Notably, both the motion of V$_O^{\bullet\bullet}$ and polarons hopping from Ce^{+3} to Ce^{+4} have a substantial effect on local lattice strain through chemical expansion as well as on polarization (20). From symmetry arguments, only those defects that are simultaneously electric and elastic dipoles can contribute to the piezoelectric effect (21). We observed evidence for charge transport in the electrical conductivity of the CGO films typical for hopping-like ion conduction below 1 kHz. The ionic conductivity greatly increases by applying higher fields (both E_{AC} and E_{DC}) (fig. S4C and fig. S12). The conductivity seems to contribute to the giant apparent dielectric permittivity ($|\varepsilon_r| \sim 10^9$) of the system when $f \to 0$. Therefore, the defect migration is enhanced by the static E_{DC} field and the quasi-static E_{AC} and contributes substantially to the large permittivity, leading to exceptionally large M and d at low frequencies. Notably, the approach for CGO with an electric field is generally also valid for other systems with centrosymmetric fluorite structures in films and bulk. We also show that piezoelectric response can be induced in a YSZ film, YSZ

and CGO ceramics, as well as CGO films prepared by a different deposition technique (figs. S13 to S15). The obtained piezoelectric coefficients of 10 to 100 pm/V in the frequency range of $f = 1$ Hz to 1 kHz are comparable to those presently used in microelectromechanical systems (MEMS) device applications with materials based on (Al,Sc)N and PZT (15), which indicates the strength of the proposed methodology.

To understand the relationship between the rearrangement of oxygen defects and the associated large low-frequency strain in the CGO films, we conducted in situ x-ray diffraction (XRD) measurements under the application of different E_{DC} electric fields. In these experiments, we directly observed partial transformation of initial highly strained cubic-like CGO [$a_{(C)} = b_{(C)} = c_{(C)} = 5.61$ Å, α = β = γ = 90° for $Z = 4$, where Z is the number of formula units in the unit cell] into a tetragonal phase [$a_{(T)} = b_{(T)} = 3.94$ Å, $c_{(T)} = 6.42$ Å, α = β = γ = 90° for $Z = 2$]. For example, there was a gradual appearance of the peak at 2θ ~ 32° when the applied electric field (0 to 1 MV/cm) was gradually increased (Fig. 4A; fig. S16; and supplementary text, section 4) (16). During the transformation, the base plane of the CGO unit cell shrinks by −0.73%, and the c axis expands by +14.39%, which results in a volume increase of +12.73% (supplementary text, section 4). These results explain and support the large positive strain observed along the electric field, applied along the crystallographic [001] direction, as well as the large compressive stress observed in the film plane. A similar electric field–induced phase transition has been reported in Y-doped ZrO_2 (YSZ) at 550°C (22). However, in our case, the effect was observed at room temperature and the resulting strains are much larger than the one reported in (22). In analogy to YSZ, the phase transition occurs because two oxygen sublattices are rearranged along the c direction in that two oxygen atoms move up and the others two move down while keeping a rotation symmetry of 2. The vertical spacings between O sites remain at $c/2$, resulting in a screw axis 4_2 along with c. This alternating shifting of O columns leads to a large expansion of the c axis. In YSZ, this mechanism was found to be triggered by a high V_O concentration (23, 24), whereas in ceria it is believed to also be associated with a high Ce′ (Ce^{3+}) concentration because in both cases (oxygen vacancy formation and the following change of host cation radii) the Coulombic attraction in the ionic matter is reduced (20).

These experimental results together with our measured dielectric data (fig. S12) indicate that a field-driven defect redistribution in the film is accompanied by a partial phase transition from a cubic to a tetragonal phase accompanied with a large volumetric increase.

These results are supported by the recent work of Zhu et al. (25), which showed experimentally and theoretically that oxygen vacancies play an essential role in the stabilization of the tetragonal phase in ceria. This suggests that the same mechanism is likely to occur in Gd-doped CeO_2, which may be even more susceptible to phase transition owing to a higher level of oxygen vacancies, leading to an electric field–driven tetragonal phase. The field-induced heterogeneity in the material is probably accompanied by Maxwell-Wagner dielectric and electromechanical effects (26), which, together with phase transition and chemical expansion (20), contribute to the field-induced strain and polarization. On the basis of the above results, the emergent piezoelectric behavior in Gd-doped ceria depends directly on the rate-dependent V_O motion on different scales (fig. S17). The selection of different aliovalent dopants and codoping, which can stabilize and control the presence of oxygen vacancies within an oxide material, could be an important strategy to generate sustainable large piezoelectricity using a similar working mechanism as demonstrated here.

We show the possibility of generating extraordinarily high piezoelectricity in intrinsically centrosymmetric nonstoichiometric oxides (fluorites) by the electric field–induced redistribution of mobile V_O. Our results show giant low-frequency piezoelectricity (up to d_{33} ~ 200,000 pm/V) in CGO films, induced by the concurrent application of alternating and static electric fields. Furthermore, we show a direct way to achieve selective electromechanical conversion in centrosymmetric materials—i.e., either pure and large electrostriction, pure and giant piezoelectricity, or mixed response under controlled electric fields. Controlling chemical expansion, phase transitions, diffusion, and redistribution of mobile ionic species in centrosymmetric ionic materials by electric field is a phenomenological concept with aims to induce large electromechanical conversion, which can be extended to other material systems. Our findings provide a paradigm shift in piezoelectricity by utilizing centrosymmetric materials with large ionic mobility, which opens up a path for a wide range of potential electromechanical, environmentally friendly, and biocompatible materials for applications in actuators and sensors.

REFERENCES AND NOTES

1. R. E. Newnham, *Properties of Materials: Anisotropy, Symmetry, Structure* (Oxford Univ. Press, 2005).
2. J. Holterman, P. Groen, *An Introduction to Piezoelectric Materials and Components* (Applied Piezo, 2012).
3. S.-E. Park, T. R. Shrout, *J. Appl. Phys.* **82**, 1804–1811 (1997).
4. F. Li *et al.*, *Science* **364**, 264–268 (2019).
5. H. Liu *et al.*, *Science* **369**, 292–297 (2020).
6. B. Jaffe, W. R. Cook, H. L. Jaffe, *Piezoelectric Ceramics* (Academic Press, 1971).
7. J. Kuwata, K. Uchino, Sh. Nomura, *Jpn. J. Appl. Phys.* **19**, 2099–2103 (1980).
8. B. Khanbabaee *et al.*, *Appl. Phys. Lett.* **109**, 222901 (2016).
9. M.-M. Yang *et al.*, *Nature* **584**, 377–381 (2020).
10. J. G. Swallow *et al.*, *Nat. Mater.* **16**, 749–754 (2017).
11. R. Korobko *et al.*, *Adv. Mater.* **24**, 5857–5861 (2012).
12. A. Kossoy *et al.*, *Phys. Rev. B* **87**, 054101 (2013).
13. R. Schmitt *et al.*, *Chem. Soc. Rev.* **49**, 554–592 (2020).
14. M. Hadad, H. Ashraf, G. Mohanty, C. Sandu, P. Muralt, *Acta Mater.* **118**, 1–7 (2016).
15. N. Setter *et al.*, *J. Appl. Phys.* **100**, 051606 (2006).
16. Materials and methods are available as supplementary materials online.
17. R. E. Newnham, V. Sundar, R. Yimnirun, J. Su, Q. M. Zhang, *J. Phys. Chem. B* **101**, 10141–10150 (1997).
18. F. A. Kröger, H. J. Vink, *Solid State Phys.* **3**, 307–435 (1956).
19. J. Faber, C. Geoffroy, A. Roux, A. Sylvestre, P. Abélard, *Appl. Phys. A* **49**, 225–232 (1989).
20. D. Marrocchelli, S. R. Bishop, H. L. Tuller, B. Yildiz, *Adv. Funct. Mater.* **22**, 1958–1965 (2012).
21. A. S. Nowick, W. R. Heller, *Adv. Phys.* **14**, 101–166 (1965).
22. A. Lai, C. A. Schuh, *Phys. Rev. Lett.* **126**, 015701 (2021).
23. B. D. C. Bell, S. T. Murphy, P. A. Burr, R. W. Grimes, M. R. Wenman, *J. Appl. Phys.* **117**, 084901 (2015).
24. H. Ikeno *et al.*, *J. Phys. Condens. Matter* **25**, 165505 (2013).
25. H. Zhu *et al.*, *Nat. Commun.* **9**, 5063 (2018).
26. G. S. Radchenko, A. V. Turik, *Phys. Solid State* **45**, 1759–1762 (2003).

Science

Induced giant piezoelectricity in centrosymmetric oxides

D.-S. ParkM. HadadL. M. RiemerR. IgnatansD. SpiritoV. EspositoV. TileliN. GauquelinD. ChezganovD. JannisJ. VerbeeckS. GorfmanN. PrydsP. MuraltD. Damjanovic

A surprising way to detect strain

Piezoelectric materials usually rely on their crystal structure alone to create electrical charge in response to strain. This makes the materials attractive for a variety of sensing applications. Park *et al.* present a different strategy by introducing gadolinium into non-piezoelectric cerium dioxide (see the Perspective by Li). This approach also creates oxygen vacancies that turn the material into one with a frequency-dependent piezoelectric effect under a static electric field. The size of the effect is similar to that of commercial piezoelectric materials, and the strategy should work more generally for a wide class of materials. —BG

View the article online
https://www.science.org/doi/10.1126/science.abm7497
Permissions
https://www.science.org/help/reprints-and-permissions

Use of this article is subject to the Terms of service